Comparison of two levels of cell models for an EV current cycle

Ronan German, J. Jaguemont, Alain Bouscayrol

Comparison of two levels of cell models for an EV current cycle

R. German[1, 3], J. Jaguemont[2,3], A. Bouscayrol[1,3]

[1] Univ. Lille, Arts et Metiers Institute of Technology, Centrale Lille, Yncrea Hauts de France, ULR2697
L2EP, F 59000 Lille, France
[2] Elektrotechniek en Energietechniek (ETEC), Vrije Universiteit Brussel, België
[3] PANDA H2020 project, Grant Agreement 824256, https://project-panda.eu/

Abstract- **This paper studies the effect of the granularity of a cell model on the voltage accuracy. A multi-coupled cell model with varying parameters is compared with a simpler one (varying voltage source and equivalent series resistance). The first model implies a very long and complex characterization process. The second one is very simple. Experiments are performed at different temperatures by applying a current profile corresponding to a driving cycle of an electric vehicle. Experimental results show both models can be used for 25°C and 10 °C ambient temperatures with reasonable accuracy. Nevertheless, when the temperature is cold the multi-coupled model is more accurate.**

Index Terms— **Multi-level Modelling; Li-ion Batteries; Electric Vehicle;**

I. INTRODUCTION

Lithium-ion battery modelling is a key-point for simulation studies of recent Electric Vehicles (EVs). The uncertainty for driving range estimation is a frequent worry for the future EV owners [1]-[3]. Different battery models are proposed in literature. But when the battery is included in global simulation at the vehicle level, most of these models are very simple [4], [5].

For an accurate EV simulation, the battery model has to deliver the right voltage for a given current profile [6]. Many parameters influence the battery voltage. The most important is the State-of-Charge (SoC), then it is the temperature [7]-[9]. Other factors of influence are the current rate [10],[11] and the direction of the current (charge-discharge hysteresis) [12].

Every publication on battery modelling in EV takes into account at least the SoC and sometimes other parameters (temperature, C-rate…). Nevertheless taking into account all of the listed dependencies results in a long and complex characterization process of the battery [13], [14].

This paper compares two models of battery cells in the perceptive to be used for vehicle simulations.

Section II presents the studied models. Section III presents the characterization results and experimental comparisons.

II. PRESENTATION OF THE STUDIED MODELS

A. Description of the two battery models

The most complex model studied in this paper is a Thevenin model (Fig. 1) for the electrical part, and a single time constant model for the thermal part (Fig. 2). The differences with a classical Thevenin model are as follows.

- The thermal part is coupled with the electrical part [8], [9]. The electrical part generates heating power by Joule effect. The thermal part reacts by modifying the cell temperature. That changes in return the value of the electrical parameters (Fig. 3).
- All of the electrical parameters are impacted by the cell temperature and the (SoC) (as in [8]) but also by other parameters such as the current rate [11] and the direction of the current [12] (charge and discharge).

The electrical part of the model is composed of 4 equivalent parameters. The open-circuit voltage (OCV_{Cell}) is an image of the available energy. The resistance R_{0Cell} represents the voltage losses due to the connections and the transport of ions. R_{1Cell} and C_{1Cell} represent the diffusion of ions into the battery electrodes. The thermal part (Fig. 2) is composed of a thermal capacitance (C_{ThCell} (J/K)) and a thermal resistance (R_{ThCell} (W/K)). The thermal capacitance represents the ability of the cell to store thermal energy. The thermal resistance represents the thermal gradient at the interface between the cell and the ambient air. This model is called the multi-coupled Thevenin model.

The second model is simpler (Fig. 4). The OCV is only dependent on the SoC. A unique Equivalent Series Resistance (ESR) represents the voltage losses. As it can be often deduced from the cell datasheets (presenting some discharge curves and an equivalent resistance): it is called the datasheet model.
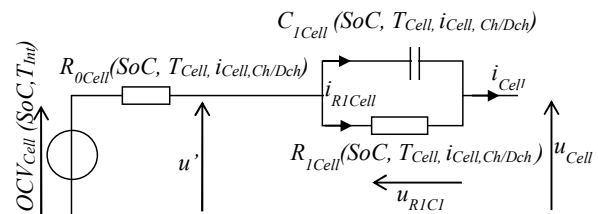

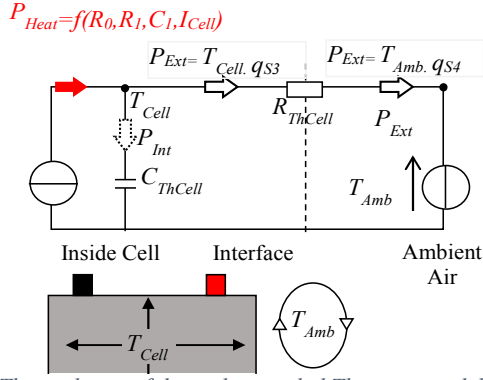Fig. 1 Electrical part of the multi-coupled Thevenin model

$P_{Heat}=f(R_0,R_1,C_1,I_{Cell})$

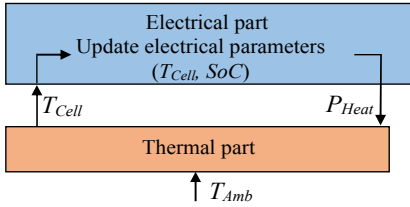Fig. 2 Thermal part of the multi-coupled Thevenin model

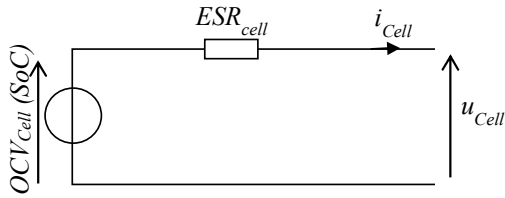

Fig. 3 Coupling between thermal and electrical parts

Fig. 4 Datasheet model

B. EMR of the battery models.

Energetic Macroscopic Representation (EMR) [15] is used to organize both models (Fig. 5, Fig. 6). EMR is a functional description based on the action-reaction principle. The functions are represented by pictograms (see Appendix). The power flows between the pictograms are obtained by multiplying the corresponding action and reaction variables [16]. EMR influences also the way of building equations. In EMR the physical causality (output delayed compared to input) is respected [17], [18]. Thus, the differential equations are re-organized with integrals.

The equation of the datasheet model are:

$$SoC_{Cell}(\%) = SoC_{Init} - \frac{100}{3600.C_{AhCell}} . \int_0^{t_{Ch/Dch}} i_{Cell}\, dt \qquad (1)$$

$$OCV_{Cell} = f(SoC_{Cell}) \qquad (2)$$

$$OCV_{Cell} - ESR_{Cell}.i_{Cell} = u_{Cell} \qquad (3)$$

Where SoC_{Cell} is the cell state of charge (in %), C_{AhCell} is the cell capacity (in Ah), ESR_{Cell} is the cell equivalent series resistance (in Ω). The open circuit voltage of the cell (OCV_{Cell}) is dependent of SoC_{Cell} with a table of values. u_{Cell} (in V) is the voltage at the cell output.
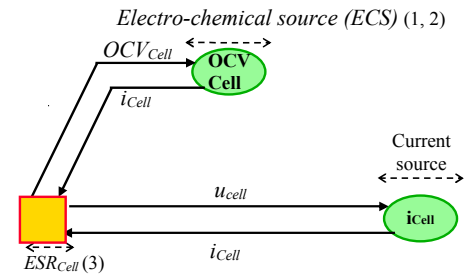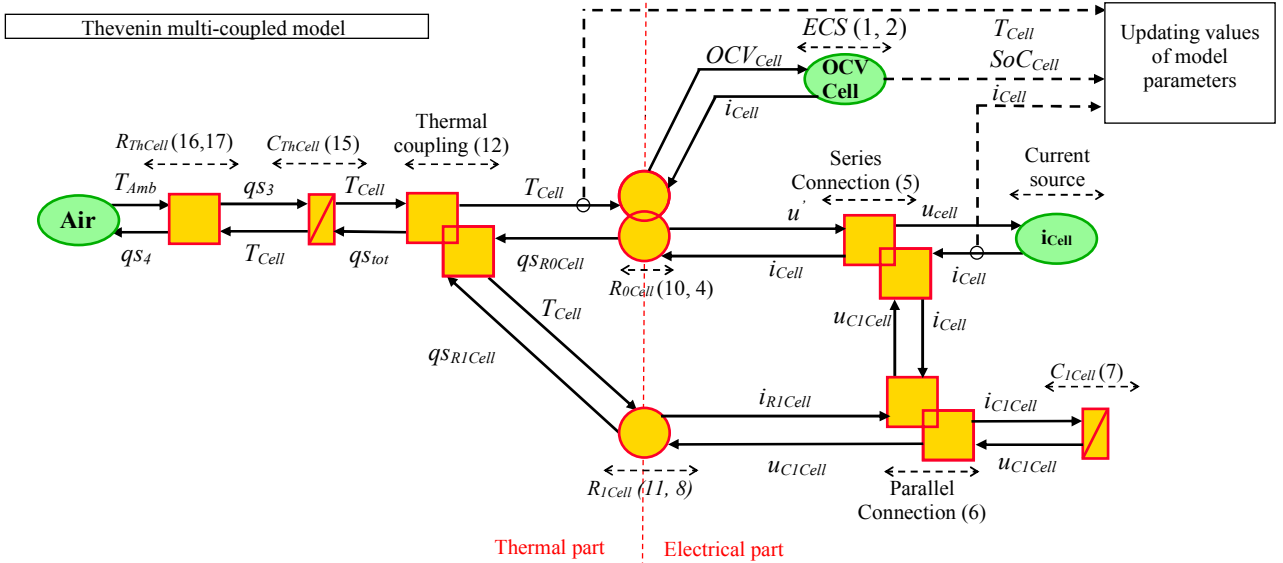

Fig. 5 EMR of the datasheet model

Fig. 6 EMR of the multi-coupled Thevenin model

The equations of the multi-coupled Thevenin model, organized in EMR (Fig. 6, Appendix), are presented below. Eq (1-2) are still valid. The next Equations (4-8) represent the electrical part of the cell model (Fig. 1). The voltage loss due to R_{0Cell}, is described by a conversion element in EMR.

$$OCV_{Cell} - R_{0Cell}.i_{Cell} = u_{Cell} \qquad (4)$$

The series connection is a power coupling element:

$$u' - u_{R1C1} = u_{Cell} \qquad (5)$$

The parallel connection (current node) is also a coupling element:

$$i_{Cell} - i_{R1Cell} = i_{C1Cell} \qquad (6)$$

C_{1Cell} is an accumulation element because there is a delay between the input (i_{C1Cell}) and the output (u_{R1C1}). It is represented with integral causality for EMR:

$$u_{R1C1} = \frac{1}{C_{1Cell}} \int_0^t i_{C1Cell} \, dt \qquad (7)$$

R_{1Cell} is a conversion element as there is no delay between inputs and outputs:

$$i_{R1Cell} = \frac{u_{R1C1}}{R_{1Cell}} \qquad (8)$$

The thermal part of the model (Fig. 2) is organized by EMR. The effort variable is the temperature (K). The flow variable is the entropy flow q_S (in W/K). The thermal power P is calculated by multiplying those two variables:

$$P = q_S.T \qquad (9)$$

The entropy flows generated by the joule effect in R_{SCell} (10) and $R_{DiffCell}$ (11) are coupled (12):

$$q_{SR0Cell} = \frac{R_{0Cell}.i_{Cell}^2}{T_{Cell}} \qquad (10)$$

$$q_{SR1Cell} = \frac{R_{1Cell}.i_{R1Cell}^2}{T_{Cell}} \qquad (11)$$

$$q_{STot} = q_{SR0Cell} + q_{R1Cell} \qquad (12)$$

In EMR, the thermal capacitance is an accumulation element, because of the differential equation (implying a delay between inputs and outputs) (13). This equation is re-organized in an integral formalism for EMR use (15). $T_{CellInit}$ is the initial internal temperature of the cell.

$$\frac{dT_{Cell}}{dt} = \frac{P_{Int}}{C_{ThCell}} \qquad (13)$$

$$\Leftrightarrow \frac{dT_{Cell}}{dt} = \frac{(q_{STotCell} - q_{S3}).T_{Cell}}{C_{ThCell}} \qquad (14)$$

$$\Leftrightarrow T_{Int} = T_{CellInit}.e^{\frac{1}{C_{ThCell}} \int_0^t (q_{STotCell} - q_{S3})dt} \qquad (15)$$

The surrounding air is imposing the ambient temperature (T_{Amb}). The thermal resistance is a conversion element (16), (17).

$$q_{S3} = \frac{T_{Int} - T_{Amb}}{(R_{ThCell}).T_{Int}} \qquad (16)$$

$$q_{S4} = \frac{T_{Int} - T_{Amb}}{(R_{ThCell}).T_{Amb}} \qquad (17)$$

As R_{0Cell} and R_{1Cell} are linked with both thermal and electrical parts, they are represented as multi-physical (electro-thermal) converters.

All of the electrical parameters (OCV_{Cell}, R_{sCell}, $R_{DiffCell}$, $C_{DiffCell}$) are dependent on the internal temperature, the current and the SoC of the cell (Fig. 6). The thermal parameters are constant, as they are related to geometry and mass of the cell.

III. EXPERIMENTAL SETUP AND RESULTS

A. Experimental characterization of the cells

The chosen cell is a NMC pouch cell (Fig. 7). This technology is widespread in EVs and HEVs. The nominal capacitance is 40 Ah. It is able to perform high current discharge (12 C = 960 A) during a few seconds.

A complete electrical characterization of the cell has been performed in [19]. Fig. 8 to Fig. 12 present the evolution of the parameters as a function of the *SoC* and the temperature in discharge for a C-rate of 0.2 C (8 A). The same characterizations are also performed:

- with higher C-rates (from 0.2 to 2C (Fig. 9)),
- in charging mode.

The goal is to obtain the evolution of the electrical parameters for all the inputs of the multi-coupled Thevenin model (see Fig. 1).

Fig. 8 presents the OCV_{Cell} evolution for different temperatures (from 10 °C to 45 °C). It appears to be few influenced by the temperature. The R_{0Cell} value increases significantly at 10°C (Fig. 10). Indeed, the cold temperature makes the ionic circulation more difficult. Thus, the resistance value is higher. ESR_{Cell} (for the datasheet model) is extracted at 50% *SoC* and 25°C as usual. It is a fixed value. Fig. 11 and Fig. 12 show that R_{1Cell} and C_{1Cell} are few affected by SoC and more by the temperature.

The thermal part of the multi-coupled Thevenin model is extracted by applying a +/-80 A square current to the cell. The square period is short (10 s) to maintain the SoC of the cell constant (50% for this experiment). During the temperature rising phase, the thermal constant is extracted. During the steady-state the thermal resistance is extracted (Fig. 13). R_{ThCell} value is 0.414 K/W and C_{ThCell} is 940 J/K.

Fig. 14 presents the validation of the thermal model at several ambient temperatures for a full cell discharge at 80 A.
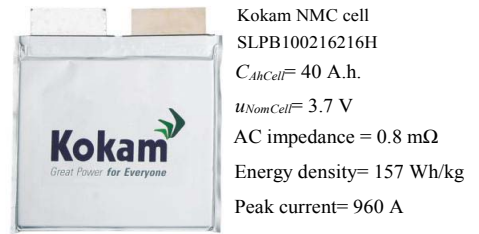

Kokam NMC cell
SLPB100216216H
C_{AhCell}= 40 A.h.
$u_{NomCell}$= 3.7 V
AC impedance = 0.8 mΩ
Energy density= 157 Wh/kg
Peak current= 960 A

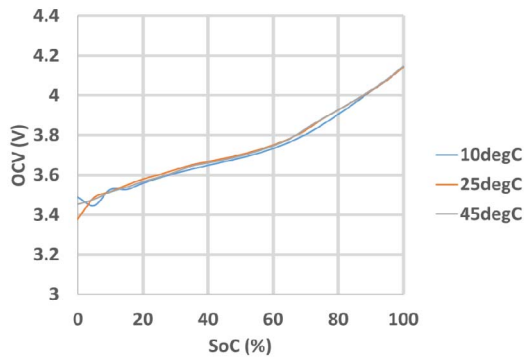*Fig. 7 Characterized NiMH Cell [20]*

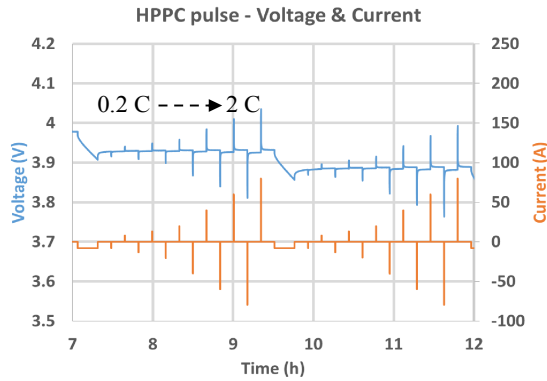Fig. 8 Evolution of the cell OCV with SoC (discharge @ 0.2C)

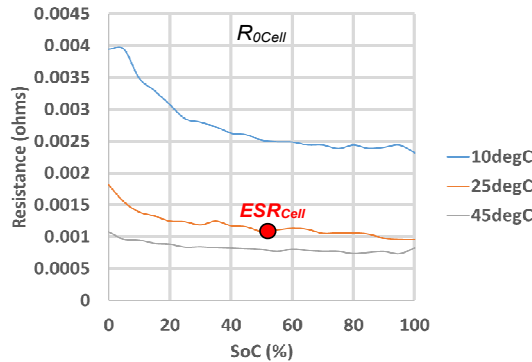Fig. 9 Impedance multi-impulsion protocol (discharge)

Fig. 10 Evolution of R_{0Cell} with SoC and temperature (for 0.2 C impulsion, in discharge)
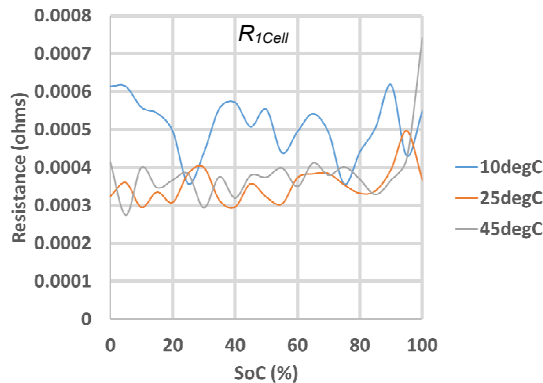

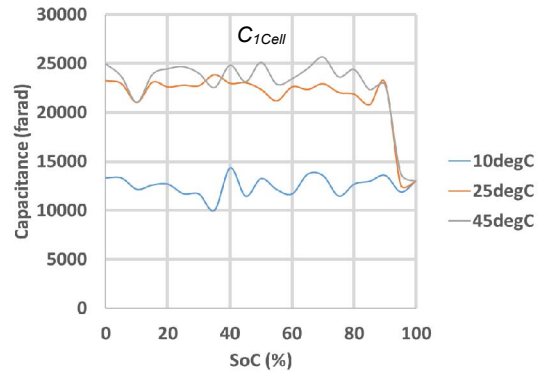Fig. 11 Evolution of R_{1Cell} with SoC and temperature (for 0.2 C impulsion, in discharge)

Fig. 12 Evolution of C_{1Cell} with SoC and temperature (for 0.2 C impulsion, in discharge)
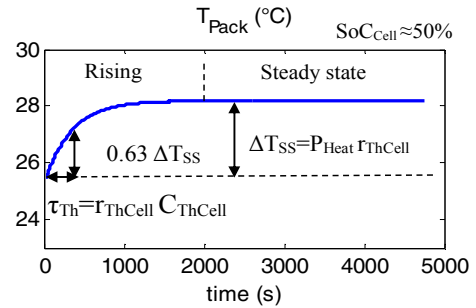

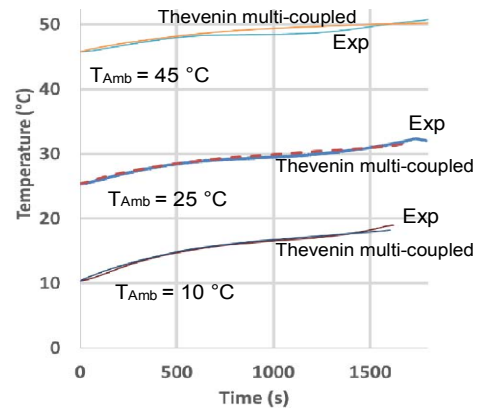
Fig. 13 Thermal characterization principle

Fig. 14 Validation of the Thevenin multi-coupled model thermal part for full discharge at 2C

B. Comparison of the models

A current profile, corresponding to several WLTC (urban and extra-urban normalized driving cycle), is applied to the tested cell (Fig. 15). The test is performed at 25°C and 10 °C as ambient temperatures. The cell is placed in a thermal chamber and is left at rest until the measured cell temperature is the same than the ambient one. The initial SoC of the cell is 90% and the final one is 40%.

The experimental results corresponding to the cell voltage are compared to the both studied models with the same current profile as input (Fig. 16).

At 25 °C, the both models give results close to the experimental ones. This is due to the contained self-heating of the cell during the test (Fig. 17).

At 10 °C the parameters of the cells are different from the datasheet one (characterized at 25 °C). As a consequence, the

multi-coupled Thevenin model is closer to the experimental cell.

The average model errors can be deduced from (4).

$$\varepsilon(\%) = \frac{\sum_1^{N_S}|u_{CellSim} - u_{CellExp}|}{N_s} \frac{100}{u_{CellNom}} \qquad (18)$$

Where N_S is the number of samples and $u_{CellNom}$ is the nominal voltage of one cell.

Fig. 19 confirms that using the both model is possible at 25 °C with errors lower than 0.5 % for the cell voltage. At 10°C the error of the datasheet model is multiplied by 3 (1.5 %). But this level of error is acceptable at the systems level for a vehicle simulation. However, for lower temperatures the error would be even bigger.
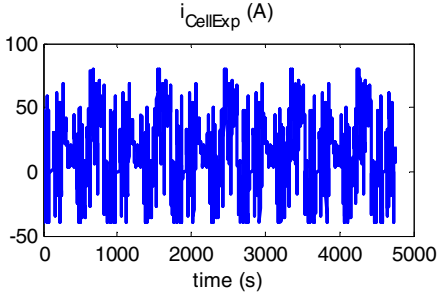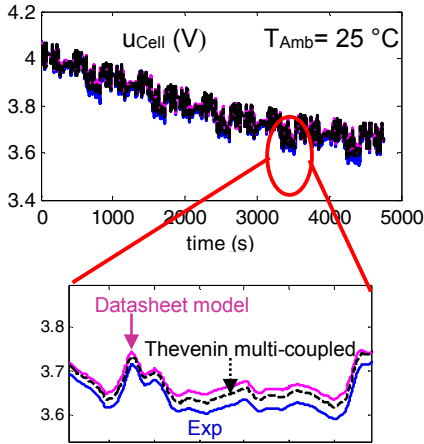

Fig. 15 Experimental EV current profile

Fig. 16 Comparison of the voltage of the two models with the experimental one for a 25 °C ambient temperature.
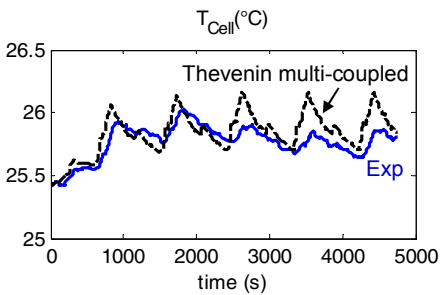

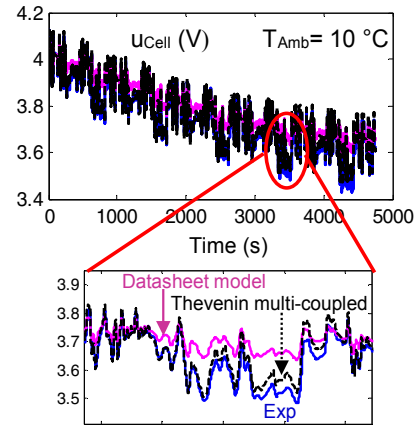*Fig. 17 Evolution of the temperature for the current profile for a 25°C ambient temperature*

Fig. 18 Comparison of the voltage of the two models with the experimental one for a 10 °C ambient temperature
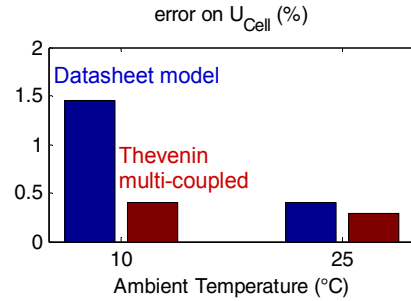

Fig. 19 Error on cell voltage for the two models for 10 °C and 25 °C temperatures

IV. CONCLUSION

This paper has presented two cells model that can be used in EV or HEV simulations.

The first one is called the datasheet model. It is composed of a voltage source dependent on the SoC and a fixed resistance. It is easy to pick up the parameters in datasheets (characterization is optional) and to simulate. The second one is a multi-coupled Thevenin model with a thermal part. Every electrical parameter are dependent on the SoC, the temperature and the current. The characterization process is long and needs equipment.

The characterization results are presented for one cell at several temperatures, SoC and current levels. The results are stored in tables.

A comparison between the experimental results and the models is performed with a normalized driving cycle current (WLTC). It shows that the simplest model can be used at warm temperature (25 °C) and medium temperature (10°C) for EV simulation studies with reasonable accuracy. Nevertheless, the multi-coupled Thevenin model could be of interest at low temperature.

As a perspective, several levels of complexity can be studied as a function of the simulation conditions. The impact of more constraining cycles (real cycles with higher current rates [9]) should be studied to specify the limits of the proposed models. Moreover lower temperature should be also studied. Finally, charging operation has also to be considered because the required higher current for a long time.
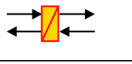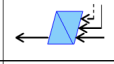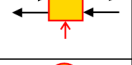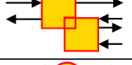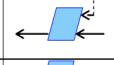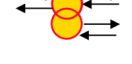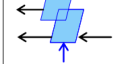
References

[1] X. Li, C. Liu, and J. Jia, « Ownership and Usage Analysis of Alternative Fuel Vehicles in the United States with the 2017 National Household Travel Survey Data », *Sustainability*, vol. 11, no 8, p. 1‑16, 2019.

[2] A. Mahmoudzadeh Andwari, A. Pesiridis, S. Rajoo, R. Martinez-Botas, and V. Esfahanian, "A review of Battery Electric Vehicle technology and readiness levels," *Renew. Sustain. Energy Rev.*, vol. 78, no. October 2015, pp. 414–430, 2017.

[3] I. Dincer, H. S. Hamut, and J. Nader, Thermal Management of Electric Vehicle Battery Systems, Wiley. 2017.

[4] C. Dépature, W. Lhomme, A. Bouscayrol, P. Sicard, L. Boulon, "Efficiency map of the traction system of an electric vehicle from an on-road test drive", *IEEE Vehicle Power and Propulsion Conference*, Coimbra (Portugal), Oct. 2014.

[5] V. Johnson, "Battery performance models in ADVISOR," Journal of Power Sources, vol. 110, pp. 321-329, 2002.

[6] G. Giordano, V. Klass, M. Behm, G. Lindbergh and J. Sjöberg, "Model-Based Lithium-Ion Battery Resistance Estimation From Electric Vehicle Operating Data," in *IEEE Transactions on Vehicular Technology*, vol. 67, no. 5, pp. 3720-3728, May 2018, doi: 10.1109/TVT.2018.2796723.

[7] A. Cappetto, W.J. Cao, J.F. Luo, M. Hagen, D. Adams, A. Shelikeri, K. Xu, J.P. Zheng,., « Performance of wide temperature range electrolytes for Li-Ion capacitor pouch cells », *J. Power Sources,* vol. 359, p. 205‑214, Aug. 2017.

[8] J. Jaguemont, L. Boulon, and Y. Dubé, « Characterization and Modeling of a Hybrid-Electric-Vehicle Lithium-Ion Battery Pack at Low Temperatures », IEEE Transactions on Vehicular Technology, vol. 65, no 1, p. 1‑14, Jan. 2016.

[9] R. German, S. Shili, A. Desreveaux, A. Sari, P. Venet and A. Bouscayrol, "Dynamical Coupling of a Battery Electro-Thermal Model and the Traction Model of an EV for Driving Range Simulation," in *IEEE Transactions on Vehicular Technology*, vol. 69, no. 1, pp. 328-337, Jan. 2020.

[10] A. Hentunen, T. Lehmuspelto and J. Suomela, "Time-Domain Parameter Extraction Method for Thévenin-Equivalent Circuit Battery Models," in *IEEE Transactions on Energy Conversion*, vol. 29, no. 3, pp. 558-566, Sept. 2014,.

[11] Y. Cao, R. C. Kroeze and P. T. Krein, "Multi-timescale Parametric Electrical Battery Model for Use in Dynamic Electric Vehicle Simulations," in *IEEE Transactions on Transportation Electrification*, vol. 2, no. 4, pp. 432-442, Dec. 2016,.

[12] F. Baronti, N. Femia, R. Saletti, C. Visone and W. Zamboni, "Hysteresis Modeling in Li-Ion Batteries," in *IEEE Transactions on Magnetics*, vol. 50, no. 11, pp. 1-4, Nov. 2014, Art no. 7300704, doi: 10.1109/TMAG.2014.2323426.

[13] A. Nikolian Joris Jaguemont, Joris de Hoog, Shovon Goutam, Noshin Omar, Peter Van Den Bossche, Joeri Van Mierlo,, "Complete cell-level lithium-ion electrical ECM model for different chemistries (NMC, LFP, LTO) and temperatures (−5 °C to 45 °C) – Optimized modelling techniques," *Int. J. Electr. Power Energy Syst.*, vol. 98, no. November 2017, pp. 133–146, 2018.

[14] J. Jaguemont, A. Nikolian, N. Omar, S. Goutam, J. Van Mierlo and P. Van den Bossche, "Development of a Two-Dimensional-Thermal Model of Three Battery Chemistries," in *IEEE Transactions on Energy Conversion*, vol. 32, no. 4, pp. 1447-1455, Dec. 2017.

[15] A. Bouscayrol, J. P. Hautier, B. Lemaire-Semail, "Graphic Formalisms for the Control of Multi-Physical Energetic Systems", Systemic Design Methodologies for Electrical Energy, tome 1, Analysis, Synthesis and Management, Chapter 3, ISTE Willey editions, October 2012, ISBN: 9781848213883

[16] A. Bouscayrol, B. Davat, B. de Fornel, B. François, J. P. Hautier, F. Meibody-Tabar, M. Pietrzak-David, "Multimachine Multiconverter System: application for electromechanical drives", European Physics Journal - Applied Physics, vol. 10, no. 2, pp. 131-147, May 2000.

[17] I. Iwasaki, H.A. Simon, "Causality and model abstraction", *Artificial Intelligence*, vol. 67, pp. 143-194, 1994

[18] J.P. Hautier, P.J. Barre, « The causal ordering graph – A tool for modeling and control law synthesis", *Studies in Informatics and Control Journal*, vol. 13, no. 4, pp. 265-283, 2004.

[19] J. Jaguemont, C. Husar, R. German, "Multi-level knowledge models of batteries", technical report, PANDA H2020 project, European commission Grant Agreement 824256, https://project-panda.eu/ ,2019.

[20] Kokam, "Kokam lithium ion cells SLPB series data", http://kokam.com/data/2019_Kokam_Cell_ver_4.2.pdf, version 4.2, 2019

Appendix: EMR Pictograms

	Source element (energy source)		Accumulation element (energy storage)		Indirect inversion (closed-loop control)
	Mono-physical conversion element		Mono-physical coupling element (energy distribution)		Direct inversion (open-loop control)
	Multi-physical conversion element		Multi-physical coupling element (energy distribution)		Coupling inversion (energy criteria)